SIAM J. SCI. COMPUT.
Vol. 36, No. 5, pp. B777–B794

FAST AND ACCURATE EVALUATION OF NONLOCAL COULOMB AND DIPOLE-DIPOLE INTERACTIONS VIA THE NONUNIFORM FFT*

SHIDONG JIANG†, LESLIE GREENGARD‡, AND WEIZHU BAO§

Abstract. We present a fast and accurate algorithm for the evaluation of nonlocal (long-range) Coulomb and dipole-dipole interactions in free space. The governing potential is simply the convolution of an interaction kernel $U(\mathbf{x})$ and a density function $\rho(\mathbf{x}) = |\psi(\mathbf{x})|^2$ for some complex-valued wave function $\psi(\mathbf{x})$, permitting the formal use of Fourier methods. These are hampered by the fact that the Fourier transform of the interaction kernel $\widehat{U}(\mathbf{k})$ has a singularity and/or $\widehat{\rho}(\mathbf{k}) \neq 0$ at the origin $\mathbf{k} = \mathbf{0}$ in Fourier (phase) space. Thus, accuracy is lost when using a uniform Cartesian grid in $\mathbf{k}$ which would otherwise permit the use of the FFT for evaluating the convolution. Here, we make use of a high-order discretization of the Fourier integral, accelerated by the nonuniform fast Fourier transform (NUFFT). By adopting spherical and polar phase-space discretizations in three and two dimensions, respectively, the singularity in $\hat{U}(\mathbf{k})$ at the origin is canceled so that only a modest number of degrees of freedom are required to evaluate the Fourier integral, assuming that the density function $(\rho\mathbf{x})$ is smooth and decays sufficiently quickly as $|\mathbf{x}| \to \infty$. More precisely, the calculation requires $O(N \log N)$ operations, where N is the total number of discretization points in the computational domain. Numerical examples are presented to demonstrate the performance of the algorithm.

Key words. Coulomb interaction, dipole-dipole interaction, interaction energy, nonuniform FFT, nonlocal, Poisson equation

AMS subject classifications. 33C10, 33F05, 44A35, 65R10, 65T50, 81Q40

DOI. 10.1137/130945582

1. Introduction.

Nonlocal (long-range) interactions are encountered in modeling a variety of problems from quantum physics and chemistry to materials science and biology. A typical example is the Coulomb interaction in the nonlinear Schrödinger equation (or Schrödinger–Poisson system in three dimensions) as a "mean field limit" for N-electrons, assuming binary Coulomb interactions [11, 12, 25] and the Kohn–Sham equation of density functional theory for electronic structure calculations in materials simulation and design [25, 40, 55, 58, 59]. Dipole-dipole interactions arise in quantum chemistry [34, 45], in dipolar Bose–Einstein condensation (BEC) [3, 4, 5, 33, 42, 48, 57, 65, 66, 67], in dipolar Fermi gases [50], and in dipole-dipole interacting Rydberg molecules [37, 38, 39].

In physical space, the interaction kernel is both long-range and singular at the origin, requiring both accurate quadrature techniques and suitable fast algorithms.

*Submitted to the journal's Computational Methods in Science and Engineering section November 18, 2013; accepted for publication (in revised form) June 23, 2014; published electronically September 30, 2014. Part of this work was done when the first and third authors were visiting Beijing Computational Science Research Center in the summer of 2013.

http://www.siam.org/journals/sisc/36-5/94558.html

†Department of Mathematical Sciences, New Jersey Institute of Technology, Newark, NJ 07102 (shidong.jiang@njit.edu). This author's research was supported by the National Science Foundation under grant CCF-0905395.

‡Courant Institute of Mathematical Sciences, New York University, New York, NY 10012 (greengard@courant.nyu.edu). This author's research was supported in part by the U.S. Department of Energy under contract DEFG0288ER25053.

§Department of Mathematics and Center for Computational Science and Engineering, National University of Singapore, Singapore 119076 (matbaowz@nus.edu.sg). This author's research was supported by the Singapore A*STAR SERC PSF-grant 1321202067.

When the density function is smooth, however, it is often more convenient to use Fourier methods since the frequency content is well controlled. Unfortunately, the Fourier transform of the interaction kernel is singular at the origin of Fourier (phase) space as well, resulting in significant numerical burdens and challenges [4, 5, 10, 14, 15, 28, 61, 69].

In this paper, we present a fast and accurate algorithm for the numerical evaluation of the interaction potential [11, 25, 40, 55, 57, 58, 65, 66, 67]

$$u(\mathbf{x}) = (U * \rho)(\mathbf{x}) := \int_{\mathbb{R}^d} U(\mathbf{x}-\mathbf{y})\rho(\mathbf{y})\, d\mathbf{y}, \qquad \mathbf{x} \in \mathbb{R}^d, \qquad d = 3, 2, \tag{1.1}$$

and its related interaction energy [11, 25, 40, 55, 57, 58, 65, 66, 67]

$$E(\rho) := \frac{\lambda}{2} \int_{\mathbb{R}^d} u(\mathbf{x})\rho(\mathbf{x})\, d\mathbf{x} = \frac{\lambda}{2} \int_{\mathbb{R}^d \times \mathbb{R}^d} \rho(\mathbf{x}) U(\mathbf{x}-\mathbf{y})\rho(\mathbf{y})\, d\mathbf{y} d\mathbf{x}, \tag{1.2}$$

where $U(\mathbf{x})$ is a nonlocal (long-range) interaction kernel and $\rho(\mathbf{x}) = |\psi(\mathbf{x})|^2$ is a density function derived from a complex-valued wave function $\psi(\mathbf{x})$. Here, λ is a dimensionless interaction constant, and $*$ denotes the convolution operator. In most applications, the density function ρ is smooth and very rapidly decaying [3, 25, 40, 55, 57, 58, 65, 66] so that it can be viewed as having compact support to a prescribed precision ε. We focus our attention on the following Coulomb and dipole-dipole interactions:

1. *Coulomb interactions in three dimensions* [8, 11, 12, 25, 36, 40, 55, 58]. The interaction kernel and its Fourier transform are given by the formulas

$$U_{\mathrm{Cou}}(\mathbf{x}) = \frac{1}{4\pi|\mathbf{x}|} \quad \Longleftrightarrow \quad \widehat{U}_{\mathrm{Cou}}(\mathbf{k}) = \frac{1}{\|\mathbf{k}\|^2}, \qquad \mathbf{x}, \mathbf{k} \in \mathbb{R}^3. \tag{1.3}$$

   In certain settings, the density is strongly confined in two dimensions, and one seeks the Coulomb potential in that plane alone. This arises in various problems of surface physics [8, 13, 20, 28], and the governing potential is obtained in two dimensions by dimension reduction from three dimensions under an anisotropic potential. This is well known to yield

$$U^{(2.5)}_{\mathrm{Cou}}(\mathbf{x}) = \frac{1}{2\pi|\mathbf{x}|} \quad \Longleftrightarrow \quad \widehat{U}^{(2.5)}_{\mathrm{Cou}}(\mathbf{k}) = \frac{1}{\|\mathbf{k}\|}, \qquad \mathbf{x}, \mathbf{k} \in \mathbb{R}^2. \tag{1.4}$$

   The superscript (2.5) is intended to denote that the sources lie in a two-dimensional (2D) space but that the physical interaction is that of the ambient three-dimensional space. Here $\widehat{f}(\mathbf{k})$ is the Fourier transform of a function $f(\mathbf{x})$ defined by the formula $\widehat{f}(\mathbf{k}) = \int_{\mathbb{R}^d} f(\mathbf{x})\, e^{-i\,\mathbf{k}\cdot\mathbf{x}}\, d\mathbf{x}$ for $\mathbf{x}, \mathbf{k} \in \mathbb{R}^d$.
2. *Dipole-dipole interactions with the same dipole orientation in three dimensions* [3, 4, 5, 9, 18, 42, 45, 51, 52, 57, 61, 65, 66, 67]. The interaction kernel is given by the formula

$$U_{\mathrm{dip}}(\mathbf{x}) = \frac{3}{4\pi} \frac{1 - 3(\mathbf{x}\cdot\mathbf{n})^2/|\mathbf{x}|^2}{|\mathbf{x}|^3} = -\delta(\mathbf{x}) - 3\,\partial_{\mathbf{nn}} \left(\frac{1}{4\pi|\mathbf{x}|} \right), \quad \mathbf{x} \in \mathbb{R}^3, \tag{1.5}$$

   and its Fourier transform is [3, 5, 42, 51, 52, 64]

$$\widehat{U}_{\mathrm{dip}}(\mathbf{k}) = -1 + \frac{3(\mathbf{n}\cdot\mathbf{k})^2}{\|\mathbf{k}\|^2}, \qquad \mathbf{k} \in \mathbb{R}^3, \tag{1.6}$$

where $\mathbf{n} = (n_1, n_2, n_3)^T$ is a fixed unit vector representing the dipole orientation, δ is the Dirac distribution function, $\partial_{\mathbf{n}} = \mathbf{n} \cdot \nabla$, and $\partial_{\mathbf{nn}} = \partial_{\mathbf{n}}(\partial_{\mathbf{n}})$. As in the Coulomb case, when the source distribution is strongly confined in two dimensions, dimension reduction from three dimensions under an anisotropic potential [3, 4, 9, 17, 56] yields

$$U_{\text{dip}}^{(2.5)}(\mathbf{x}) = -\alpha\,\delta(\mathbf{x}) - \frac{3}{2}\left(\partial_{\mathbf{n}_\perp\mathbf{n}_\perp} - n_3^2\Delta_\perp\right)\left(\frac{1}{2\pi|\mathbf{x}|}\right), \qquad \mathbf{x} \in \mathbb{R}^2, \tag{1.7}$$

and its Fourier transform is [3, 9, 17, 56]

$$\widehat{U}_{\text{dip}}^{(2.5)}(\mathbf{k}) = -\alpha + \frac{3\left[(\mathbf{n}_\perp \cdot \mathbf{k})^2 - n_3^2\|\mathbf{k}\|^2\right]}{2\|\mathbf{k}\|}, \qquad \mathbf{k} \in \mathbb{R}^2, \tag{1.8}$$

where $\mathbf{n}_\perp = (n_1, n_2)^T$, $\partial_{\mathbf{n}_\perp} = \mathbf{n}_\perp \cdot \nabla_\perp$, $\partial_{\mathbf{n}_\perp\mathbf{n}_\perp} = \partial_{\mathbf{n}_\perp}(\partial_{\mathbf{n}_\perp})$, $\nabla_\perp = (\partial_x, \partial_y)^T$, $\Delta_\perp = \partial_{xx} + \partial_{yy}$, and α is a fixed real constant [3, 17].

3. *Dipole-dipole interactions with different dipole orientations in three dimensions* [34, 45, 51, 52, 54]. The interaction kernel is

$$\begin{aligned} U_{\text{dip}}(\mathbf{x}) &= \frac{3}{4\pi}\frac{\mathbf{m}\cdot\mathbf{n} - 3(\mathbf{x}\cdot\mathbf{n})(\mathbf{m}\cdot\mathbf{x})/|\mathbf{x}|^2}{|\mathbf{x}|^3} \\ &= -(\mathbf{m}\cdot\mathbf{n})\delta(\mathbf{x}) - 3\,\partial_{\mathbf{nm}}\left(\frac{1}{4\pi|\mathbf{x}|}\right), \qquad \mathbf{x} \in \mathbb{R}^3, \end{aligned} \tag{1.9}$$

and its Fourier transform is [34, 45, 51, 52, 54]

$$\widehat{U}_{\text{dip}}(\mathbf{k}) = -(\mathbf{m}\cdot\mathbf{n}) + \frac{3(\mathbf{n}\cdot\mathbf{k})(\mathbf{m}\cdot\mathbf{k})}{\|\mathbf{k}\|^2}, \qquad \mathbf{k} \in \mathbb{R}^3, \tag{1.10}$$

where $\mathbf{n} = (n_1, n_2, n_3)^T$ and $\mathbf{m} = (m_1, m_2, m_3)^T$ are two fixed unit vectors representing the two dipole orientations, $\partial_{\mathbf{m}} = \mathbf{m} \cdot \nabla$, and $\partial_{\mathbf{nm}} = \partial_{\mathbf{n}}(\partial_{\mathbf{m}}) = \partial_{\mathbf{m}}(\partial_{\mathbf{n}})$. Again, when the source distribution is strongly confined in two dimensions, dimension reduction from three dimensions under an anisotropic potential [3, 4, 9, 17, 56] yields

$$U_{\text{dip}}^{(2.5)}(\mathbf{x}) = -\alpha\,\delta(\mathbf{x}) - \frac{3}{2}\left(\partial_{\mathbf{n}_\perp\mathbf{m}_\perp} - n_3m_3\Delta_\perp\right)\left(\frac{1}{2\pi|\mathbf{x}|}\right), \qquad \mathbf{x} \in \mathbb{R}^2, \tag{1.11}$$

and its Fourier transform is [3, 9, 17, 56]

$$\widehat{U}_{\text{dip}}^{(2.5)}(\mathbf{k}) = -\alpha + \frac{3\left[(\mathbf{n}_\perp \cdot \mathbf{k})(\mathbf{m}_\perp \cdot \mathbf{k}) - n_3m_3\|\mathbf{k}\|^2\right]}{2\|\mathbf{k}\|}, \qquad \mathbf{k} \in \mathbb{R}^2, \tag{1.12}$$

where $\mathbf{m}_\perp = (m_1, m_2)^T$, $\partial_{\mathbf{m}_\perp} = \mathbf{m}_\perp \cdot \nabla_\perp$, $\partial_{\mathbf{n}_\perp\mathbf{m}_\perp} = \partial_{\mathbf{n}_\perp}(\partial_{\mathbf{m}_\perp}) = \partial_{\mathbf{m}_\perp}(\partial_{\mathbf{n}_\perp})$, and α is a fixed real constant [3, 17].

Remark 1.1. Note that the second category above is a special case of the third. It is listed separately because it is simpler and has some important physical applications.

Various numerical methods have been proposed in the literature for evaluating the interaction potential (1.1) and interaction energy (1.2) using a uniform grid on a bounded computational domain so as to compute the ground states and dynamics of problems in quantum physics and chemistry. Existing schemes often use the

(uniform) FFT and ignore the singularity at the origin in $\mathbf{k}$-space, where $\widehat{U}_{\rm Cou}(\mathbf{k})$ is unbounded and $\widehat{U}_{\rm dip}(\mathbf{k})$ is nonsmooth. Unfortunately, this approach leads to very slow convergence (a phenomenon known as "numerical locking" in the literature) [5, 10, 15, 51, 52, 54, 61, 62, 64, 65, 67, 69].

As a result, there has been some interest in reformulating the problem of convolution with the three-dimensional (3D) Coulomb kernel (1.3) in terms of the governing partial differential equation (the Poisson equation)

$$-\Delta u_{\rm Cou}(\mathbf{x}) = \rho(\mathbf{x}), \qquad \mathbf{x} \in \mathbb{R}^3, \qquad \lim_{|\mathbf{x}|\to\infty} u_{\rm Cou}(\mathbf{x}) = 0, \tag{1.13}$$

and convolution with the reduced 2.5-dimensional (2.5D) Coulomb kernel (1.4) in terms of the fractional partial differential equation

$$(-\Delta)^{1/2} u_{\rm Cou}(\mathbf{x}) = \rho(\mathbf{x}), \qquad \mathbf{x} \in \mathbb{R}^2, \qquad \lim_{|\mathbf{x}|\to\infty} u_{\rm Cou}(\mathbf{x}) = 0. \tag{1.14}$$

The dipole-dipole interaction in three dimensions (1.5) can be computed from the relation [4, 5, 8, 9, 17, 69]

$$u(\mathbf{x}) = -\rho(\mathbf{x}) + 3\partial_{\mathbf{nn}} u_{\rm Cou}(\mathbf{x}), \qquad \mathbf{x} \in \mathbb{R}^3. \tag{1.15}$$

There is a substantial literature on solving the partial differential equations (1.13) and (1.14) by truncating them on a bounded computational domain with a homogeneous Dirichlet boundary condition and then discretizing them by a spectral method with sine basis via the discrete sine transformation (DST) [4, 5, 8, 9, 17]. With this method, the accuracy can be improved to six significant digits in practical computations [4, 5, 8, 9, 17]. For more details, we refer the interested reader to [4, 5, 8, 9, 17, 35, 41, 69] and the references therein. It is important to note, however, that when the density function ρ has complicated local structure, an adaptive grid is needed for resolution. In that setting, Fourier methods are highly inefficient, and the fast multipole method (FMM) or some variant [19, 28, 29, 31, 32, 68] should be used for evaluating the nonlocal interaction directly in physical space in $O(N)$ time, where N is the number of grid points. (For uniform grids, the constant in the FMM makes the present approach more attractive.)

In many applications, however, such as the computation of the ground state and dynamics of BEC [4, 5, 9, 15, 17, 61, 65, 66, 67], one needs to evaluate $u(\mathbf{x})$ on an equispaced grid in physical space many times for different $\rho(\mathbf{x})$. This occurs, for example, in time-splitting spectral methods for computing the dynamics of the nonlinear Schrödinger/Gross–Pitaevskii equations [4, 5, 6, 7]. In such cases, Fourier methods can be very efficient, easy to implement, and high-order accurate, so long as care is taken in discretization. In fact, based on the discussion above, we note that in Fourier space, the Coulomb or dipole-dipole interaction potential (1.1) is given by

$$u(\mathbf{x}) = \frac{1}{(2\pi)^d} \int_{\mathbb{R}^d} e^{i\,\mathbf{k}\cdot\mathbf{x}}\, \widehat{U}(\mathbf{k})\, \widehat{\rho}(\mathbf{k})\, d\mathbf{k}, \qquad \mathbf{x} \in \mathbb{R}^d, \qquad d = 2, 3, \tag{1.16}$$

where $\widehat{U}(\mathbf{k})$ is given by one of the formulae

(1.17)
$$\widehat{U}(\mathbf{k}) = \begin{cases} \dfrac{1}{\|\mathbf{k}\|^2}, & \text{3D Coulomb interactions,} \\ -(\mathbf{m}\cdot\mathbf{n}) + \dfrac{3(\mathbf{n}\cdot\mathbf{k})(\mathbf{m}\cdot\mathbf{k})}{\|\mathbf{k}\|^2}, & \text{3D dipole-dipole interactions,} \\ \dfrac{1}{\|\mathbf{k}\|}, & \text{2.5D Coulomb interactions,} \\ -\alpha + \dfrac{3\left[(\mathbf{n}_\perp\cdot\mathbf{k})(\mathbf{m}_\perp\cdot\mathbf{k}) - n_3 m_3\|\mathbf{k}\|^2\right]}{2\|\mathbf{k}\|}, & \text{2.5D dipole-dipole interactions.} \end{cases}$$

The remainder of this paper is aimed at the construction of a fast and accurate algorithm for the evaluation of long-range interactions of the form (1.1) as well as the total interaction energy (1.2). There are three essential ingredients. First, we truncate the integrals in (1.16) at a frequency beyond which the contribution to ρ is negligible. This is valid because of our assumption that ρ is smooth. Second, we rewrite (1.16) using spherical or polar coordinates in three dimensions or two dimensions, respectively. The Jacobian of this change of variables cancels the singularity at the origin in Fourier space, permitting the use of simple high-order quadrature rules. More precisely, we achieve superalgebraic convergence by using the trapezoidal rule in the azimuthal direction and Gauss–Legendre quadrature in the radial and inclination directions. Third, we utilize the nonuniform fast Fourier transform (NUFFT) (see, for example, [14, 22, 24, 26, 27, 30, 43, 53]) to accelerate the calculation of the sums which arise from discretization, which do not correspond to uniform tensor product grids. The resulting algorithm is high-order accurate and requires only $O(N \log N)$ operations, where N is the total number of discretization points in physical space.

The paper is organized as follows. In section 2, we present a brief review of NUFFT, and in section 3, we describe the numerical algorithm in detail. The performance of the method is illustrated with several numerical examples in section 4. Section 5 contains some concluding remarks.

2. Brief review of the NUFFT. In this section, we summarize the basic steps of the NUFFT to make the discussion reasonably self-contained.

The ordinary FFT computes the discrete Fourier transform (DFT) and its inverse:

(2.1)
$$F(k) = \sum_{j=0}^{N-1} f(j) e^{-2\pi i k j/N}, \qquad k = 0, \ldots, N-1,$$
$$f(j) = \frac{1}{N} \sum_{k=0}^{N-1} F(k) e^{2\pi i k j/N}, \quad j = 0, \ldots, N-1,$$

in $O(N \log N)$ operations by exploiting the algebraic structure of the DFT matrix. The points $x_j = 2\pi j/N$ and the frequencies k, however, must be equispaced in both the physical and Fourier domains (see, for example, [21, 60]).

The purpose of the NUFFT is to remove this restriction, while maintaining a computational complexity of $O(N \log N)$, where N denotes the total number of points in both the physical and Fourier domains. Dutt and Rokhlin were the first to construct an algorithm of this type, with full control of precision [22], although heuristic versions had been used earlier. There are, by now, many variants of the NUFFT (see, for example, [14, 22, 24, 26, 27, 30, 43, 53]). All of these algorithms rely on interpolation

coupled with a judicious use of the FFT on an oversampled grid. Here, we will follow the discussion in the paper [30], which describes a simple framework for the NUFFT using Gaussian kernels for interpolation.

The type-1 NUFFT evaluates sums of the form

$$f(\mathbf{x}) = \frac{1}{N} \sum_{n=0}^{N-1} F_n e^{-i\mathbf{k}_n \cdot \mathbf{x}} \tag{2.2}$$

for "targets" $\mathbf{x}$ on a regular grid in $\mathbb{R}^d$, given function values F_n prescribed at arbitrary locations $\mathbf{k}_n$ in the dual space. Here, N denotes the total number of source points.

The type-2 NUFFT evaluates sums of the form

$$F(\mathbf{k}_n) = \sum_{j_1=-M_1/2}^{M_1/2-1} \cdots \sum_{j_d=-M_d/2}^{M_d/2-1} f(\mathbf{x}_j) e^{-i\mathbf{k}_n \cdot \mathbf{x}_j}, \tag{2.3}$$

where the "targets" $\mathbf{k}_n$ are irregularly located points in $\mathbb{R}^d$, given the function values $f(\mathbf{x}_j)$ on a regular grid in the dual space. (The type-3 NUFFT permits the sampling to be irregular in both domains and will not be needed in the present paper.)

We now briefly explain the basic idea underlying the NUFFT [22, 30]. For simplicity, let us consider the one-dimensional (1D) type-1 NUFFT:

$$F(k) = \frac{1}{N} \sum_{j=0}^{N-1} f_j e^{-ikx_j}, \qquad k = -\frac{M}{2}, \ldots, \frac{M}{2} - 1. \tag{2.4}$$

Note now that (2.4) describes the exact Fourier coefficients of the function

$$f(x) = \sum_{j=0}^{N-1} f_j \delta(x - x_j), \tag{2.5}$$

viewed as a periodic function on $[0, 2\pi]$. Here $\delta(x)$ denotes the Dirac function. It is clearly not well resolved by a uniform mesh in x. By convolving with a heat kernel, however, we will construct a smooth function which can be sampled. For this, we let $g_\tau(x) = \sum_{l=-\infty}^{\infty} e^{-(x-2l\pi)^2/4\tau}$ denote the 1D periodic heat kernel on $[0, 2\pi]$. If we define f_τ to be convolution of f with g_τ:

$$f_\tau(x) = f * g_\tau(x) = \int_0^{2\pi} f(y) g_\tau(x - y) dy\,,$$

then f_τ is a 2π-periodic C^∞ function and is well resolved by a uniform mesh in x whose spacing is determined by τ. Thus, its Fourier coefficients $F_\tau(k) = \frac{1}{2\pi} \int_0^{2\pi} f_\tau(x) e^{-ikx} dx$ can be computed with high accuracy using the standard FFT on a sufficiently fine grid. That is,

$$F_\tau(k) \approx \frac{1}{M_r} \sum_{m=0}^{M_r-1} f_\tau(2\pi m/M_r) e^{-ik2\pi m/M_r}, \tag{2.6}$$

where

$$f_\tau(2\pi m/M_r) = \sum_{j=0}^{N-1} f_j g_\tau(2\pi m/M_r - x_j). \tag{2.7}$$

Once the values $F_\tau(k)$ are known, an elementary calculation shows that

$$F(k) = \sqrt{\frac{\pi}{\tau}} e^{k^2\tau} F_\tau(k). \tag{2.8}$$

This is a direct consequence of the convolution theorem and the fact that the Fourier transform of g_τ is $G_\tau(k) = \sqrt{2\tau} e^{-k^2\tau}$.

Optimal selection of the parameters in the algorithm requires a bit of analysis, which we omit here. We simply note [30] that if $M_r = 2M$ and $\tau = 12/M^2$, and one uses a Gaussian to spread each source to the nearest 24 grid points, then the NUFFT yields about 12 digits of accuracy. With $\tau = 6/M^2$ and Gaussian spreading of each source to the nearest 12 grid points, the NUFFT yields about 6 digits of accuracy. The type-2 NUFFT is computed by essentially reversing the steps of the type-1 NUFFT.

3. Numerical algorithms. We turn now to a detailed description of our numerical algorithms for evaluating the nonlocal (long-range) interactions (1.1) and the related interaction energy (1.2).

3.1. High-order discretization. Since we have assumed that the function ρ is smooth and rapidly decaying, we treat it as compactly supported with some prescribed precision ε in the rectangular box $B = [-R_1/2, R_1/2] \times \cdots \times [-R_d/2, R_d/2]$. Its Fourier transform $\widehat{\rho}$ is

$$\widehat{\rho}(\mathbf{k}) = \int_B e^{-i\mathbf{k}\cdot\mathbf{x}} \rho(\mathbf{x}) d\mathbf{x}, \tag{3.1}$$

where $\mathbf{x} = (x_1, \ldots, x_d)$, $\mathbf{k} = (k_1, \ldots, k_d)$.

Let us now be more specific about our smoothness assumption. We let $\rho \in C^n(B)$ so that $\widehat{\rho} = O(\|\mathbf{k}\|^{-n})$ as $\|\mathbf{k}\| \to \infty$. A straightforward calculation shows that to achieve a truncation error of ε, evaluation of (1.1) needs to be done only for $\|\mathbf{k}\| \le P$, where $P = O(1/\varepsilon)^{1/n}$. We will refer to P as the high-frequency cutoff. This fixes the range of integration in $\mathbf{k}$-space and bounds the oscillatory behavior of the term $e^{-i\mathbf{k}\cdot\mathbf{x}}$ in the integrand of (3.1).

Together with the fact that $\rho(\mathbf{x})$ is smooth, it follows that the tensor product trapezoidal rule applied to (3.1) with N_j points along the jth axis will yield $O(N^{-n})$ accuracy, where $N = \min_{j=1}^d N_j$. The error will decay rapidly once each of the N_j is of the order (PR_j) so that the integrand is well resolved. If $\rho(\mathbf{x})$ is given on a uniform mesh with N_j points in the jth dimension, the trapezoidal rule yields

$$\widehat{\rho}(\mathbf{k}) \approx \left(\prod_{j=1}^d \frac{R_j}{N_j} \right) \sum_{n_1=0}^{N_1-1} \cdots \sum_{n_d=0}^{N_d-1} e^{-i\mathbf{k}\cdot\mathbf{x}_n} \rho(\mathbf{x}_n), \tag{3.2}$$

where $\mathbf{x}_n = (-R/2 + n_1(R/N_1), \ldots, -R/2 + n_d(R/N_d))$.

To compute the desired solution in physical space, we need to evaluate the inverse Fourier transform defined by (1.16) for each of the kernels in (1.17). As discussed above, we can truncate the domain of integration in the Fourier domain at $\|\mathbf{k}\| = P = O(1/\varepsilon)^{1/n}$, with an error ε. Thus, the main issue is the design of a high-order rule for finite Fourier integrals of the form

$$u(\mathbf{x}) \approx \frac{1}{(2\pi)^d} \int_{\|\mathbf{k}\| \le P} e^{i\mathbf{k}\cdot\mathbf{x}} \widehat{U}(\mathbf{k}) \widehat{\rho}(\mathbf{k}) d\mathbf{k}. \tag{3.3}$$

The principal difficulty is that the integrand above is singular at the origin using Cartesian coordinates in $\mathbf{k}$-space. It is, however, perfectly smooth in spherical coordinates or polar coordinates, respectively. Indeed, using the usual change of variables in (3.3), we obtain

(3.4)
$$u(\mathbf{x}) \approx \frac{1}{(2\pi)^d} \begin{cases} \displaystyle\int_0^P \int_0^\pi \int_0^{2\pi} e^{i\mathbf{k}\cdot\mathbf{x}} \|\mathbf{k}\|^2 \widehat{U}(\mathbf{k}) \widehat{\rho}(\mathbf{k}) \sin\theta dk d\theta d\phi & \text{in three dimensions,} \\ \displaystyle\int_0^P \int_0^{2\pi} e^{i\mathbf{k}\cdot\mathbf{x}} \|\mathbf{k}\| \widehat{U}(\mathbf{k}) \widehat{\rho}(\mathbf{k}) dk d\phi & \text{in two dimensions.} \end{cases}$$

It is easy to see that the integrand is smooth in both integrals in (3.4) since the factor $\|\mathbf{k}\|^{d-1}$ $(d = 2, 3)$ cancels the singularity in $\widehat{U}(\mathbf{k})$ by inspection of (1.17). $\widehat{\rho}(\mathbf{k})$, of course, is smooth since it is a band-limited function.

The integrals in (3.4) can be discretized with high-order accuracy by using standard (shifted and scaled) Gauss–Legendre quadrature in the radial direction (and the longitudinal θ direction in three dimensions) combined with the trapezoidal rule for the azimuthal ϕ variable (see Figure 1). Thus, we have

(3.5)
$$u(\mathbf{x}) \approx \frac{1}{(2\pi)^d} \begin{cases} \displaystyle\sum_{j_1=1}^{N_r} \sum_{j_2=1}^{N_\theta} \sum_{j_3=1}^{N_\phi} w_j e^{i\mathbf{k}_j\cdot\mathbf{x}} \|\mathbf{k}_j\|^2 \widehat{U}(\mathbf{k}_j) \widehat{\rho}(\mathbf{k}_j) & \text{in three dimensions,} \\ \displaystyle\sum_{j_1=1}^{N_r} \sum_{j_2=1}^{N_\phi} w_j e^{i\mathbf{k}_j\cdot\mathbf{x}} \|\mathbf{k}_j\| \widehat{U}(\mathbf{k}_j) \widehat{\rho}(\mathbf{k}_j) & \text{in two dimensions.} \end{cases}$$

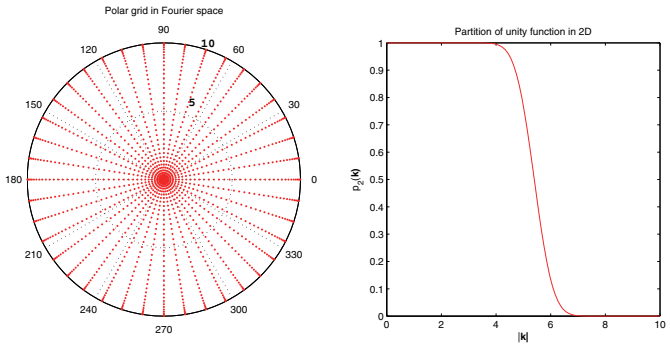

FIG. 1. *A polar grid in the Fourier domain (left) and the partition of unity function* $p_2(\mathbf{k})$ *as a function* $|\mathbf{k}|$ *(right).*

3.2. A simple procedure. It is clear that $\widehat{\rho}(\mathbf{k}_j)$ can be evaluated from (3.2) at the desired nonequispaced points $\mathbf{k}_j$ using the type-2 NUFFT. The summations defined in (3.5) can then be evaluated using the type-1 NUFFT since the desired output points $\mathbf{x}$ lie on a uniform grid in physical space.

ALGORITHM 1. Simple procedure for the evaluation of (1.16).

Given the dimension d, the box size parameters R_j, $j = 1, \ldots, d$, and the number of equispaced points N_j in each direction, compute $u(\mathbf{x})$ defined in (1.16) *on a uniform grid in $B = \prod_{j=1}^{d}[-R_j/2, R_j/2]$.*

1: Compute the coordinates on the uniform grid in B, that is, $\mathbf{x}_n = (-R_1/2 + n_1(R_1/N_1), \ldots, -R_d/2 + n_d(R_d/N_d))$, $n_j = 0, \ldots, N_j$, $j = 1, \ldots, d$.
2: Evaluate the function $\rho(\mathbf{x}_n)$ at these uniform grid points.
3: Compute the Gauss–Legendre nodes and weights r_j, w_{r_j}, $j = 1, \ldots, N_r$ for the r direction, the trapezoidal nodes ϕ_l, $l = 1, \ldots, N_\phi$ for the ϕ direction, and the Gauss–Legendre nodes and weights θ_k, w_{θ_k}, $k = 1, \ldots, N_\theta$ for the θ direction if $d = 3$.
4: Use the type-2 NUFFT to evaluate $\widehat{\rho}$ at these nonuniform grid points.
5: Use the type-1 NUFFT to evaluate $u(\mathbf{x}_n)$ defined in (3.5).

The total computational cost of Algorithm 1 is $O(N_f)+O(N_p \log N_p)$, where N_f is the total number of irregular points in the Fourier domain and N_p is the total number of equispaced points in the physical domain. As discussed at the end of section 2, the constant in front of N_f is 24^d for 12 digit accuracy with d the dimension of the problem. Since N_f is often comparable with N_p and the constant in the standard FFT is quite small, the $O(N_f)$ term will dominate the computational cost in Algorithm 1, making it considerably slower than the standard FFT.

3.3. A more elaborate algorithm. We now construct a more elaborate algorithm to reduce the interpolation cost of the preceding scheme by reducing the number of irregular points N_f.

We note that the only singular point in the Fourier domain is the origin. Thus we will split the integral in (3.3) into two parts using a simple partition of unity.

$$\begin{aligned} u(\mathbf{x}) &\approx \frac{1}{(2\pi)^d}\int_{\|\mathbf{k}\|\le P} e^{i\mathbf{k}\cdot\mathbf{x}}\widehat{U}(\mathbf{k})\widehat{\rho}(\mathbf{k})d\mathbf{k} \\ &= \int_{\|\mathbf{k}\|\le P} e^{i\mathbf{k}\cdot\mathbf{x}}\frac{\widehat{U}(\mathbf{k})}{(2\pi)^d}\widehat{\rho}(\mathbf{k})(1-p_d(\mathbf{k}))d\mathbf{k} + \int_{\|\mathbf{k}\|\le P} e^{i\mathbf{k}\cdot\mathbf{x}}\frac{\widehat{U}(\mathbf{k})}{(2\pi)^d}\widehat{\rho}(\mathbf{k})p_d(\mathbf{k})d\mathbf{k} \\ &:= I_1 + I_2. \end{aligned} \tag{3.6}$$

We now choose the function p_d so that it is a monotone C^∞ function which decays rapidly and so that $\frac{1-p_d(\mathbf{k})}{\|\mathbf{k}\|^{d-1}}$ is a smooth function for $\mathbf{k} \in \mathbb{R}^d$. By the second property of p_d, it is easy to see that I_1 can be computed using the regular FFT. If p_d decays much faster than $\hat{f}$, then I_2 can be computed using the NUFFT but with many fewer irregular points in the Fourier domain. There are many choices for p_d. Indeed, any partition of unity function that is C^∞ in $\mathbb{R}^d$ equals to 1 for $\|\mathbf{k}\| < R_0$, and 0 for $\|\mathbf{k}\| > R_1$ would work theoretically. In order to minimize the oversampling factor in the evaluation of I_1, for the 2D problems listed in (1.16) and (1.17), we choose p_2 as follows:

$$p_2(\mathbf{k}) = \frac{1}{2}\mathrm{erfc}\left(\frac{12(\|\mathbf{k}\| - (R_0+R_1)/2)}{R_1 - R_0}\right), \tag{3.7}$$

where erfc is the complementary error function defined by the formula $\mathrm{erfc}(x) = \frac{2}{\sqrt{\pi}}\int_x^\infty e^{-t^2}dt$.

Remark 3.1. Dimensional analysis indicates that R_0 and R_1 in the definition of

p_2 (3.7) should be proportional to $O(\min(\Delta k_1, \Delta k_2)) = O(1/\max(h_1, h_2))$, where h_i $(i = 1, 2)$ is the mesh size in the ith direction. Our numerical experiments show that with $R_0 = 0.8/\max(h_1, h_2)$ and $R_1 = 10/\max(h_1, h_2)$, an oversampling factor of 3 for I_1 and a 60×60 irregular grid for I_2 yield 12 digit accuracy. An oversampling factor of 2 for I_1 and a 40×40 irregular grid for I_2 yield 6 digits of accuracy. We have not carried out a more detailed optimization.

For 3D problems, we choose a simple Gaussian:

$$p_3(\mathbf{k}) = e^{-\frac{\|\mathbf{k}\|^2}{a}}. \tag{3.8}$$

It is straightforward to verify that $\frac{1-p_3(\mathbf{k})}{\|\mathbf{k}\|^2}$ has a power series expansion in $\|\mathbf{k}\|^2$, so that it is a smooth function of $\mathbf{k}$ satisfies the second property.

Remark 3.2. We still need to choose the parameter a in (3.8). Obviously, one would need fewer irregular points for I_2 if a were small, reducing the computational cost of I_2. However, the Gaussian becomes more sharply peaked, and one would need to oversample the regular grid in I_1 in order to maintain high accuracy, increasing the computational cost. Thus, a should be chosen to balance the contributions of the two integral to the net cost. Dimensional analysis indicates that a should be of the order

$$O(\min(\Delta k_1^2, \Delta k_2^2, \Delta k_3^2)) = O(1/\max(h_1^2, h_2^2, h_3^2)),$$

where the h_i $(i = 1, 2, 3)$ are the mesh size in the ith coordinate direction in physical space. Numerical experiments show that with $a = 2/\max(h_1^2, h_2^2, h_3^2)$, the oversampling factor for I_1 can be set to 2. An irregular (spherical) $40 \times 40 \times 40$ grid in the Fourier domain achieves 12 digits of accuracy for I_2, and an irregular $24 \times 24 \times 24$ grid in the Fourier domain achieves 6 digits of accuracy for I_2.

ALGORITHM 2. An improved algorithm for the evaluation of (1.16).

Given the dimension d, the box size parameters R_j, $j = 1, \ldots, d$, and the number of equispaced points N_j in each direction, compute $u(\mathbf{x})$ defined in (1.16) *on a uniform grid in $B = \prod_{j=1}^{d}[-R_j/2, R_j/2]$.*

1: Compute the coordinates of the uniform grid in B, that is, $\mathbf{x}_n = (-R_1/2 + n_1(R_1/N_1), \ldots, -R_d/2 + n_d(R_d/N_d))$, $n_j = 0, \ldots, N_j$, $j = 1, \ldots, d$.
2: Evaluate the values of the function $\rho(\mathbf{x}_n)$ at these uniform grid points.
3: Set the oversampling factor to 2, and compute I_1 in (3.6) using the regular FFT.
4: Use NUFFT as in Algorithm 1 to compute I_2 in (3.6).
5: Compute $u = I_1 + I_2$.

Remark 3.3. Once $u(\mathbf{x})$ has been computed via Algorithm 2, the interaction energy (1.2) can be discretized via the trapezoidal rule and evaluated by pointwise multiplication and direct summation in physical space. The computational cost is obviously linear in the total number of discretization points in physical space.

Remark 3.4. The computational cost of the interpolation procedure within the NUFFT has been reduced to $O(1)$ in Algorithm 2.

Remark 3.5. Our algorithm can easily be modified to evaluate any nonlocal interaction with a convolution structure, so long as the Fourier transform of the kernel is known. If the singularity at the origin of $\mathbf{k}$-space cannot be removed by switching to polar or spherical coordinates, one can easily develop a high-order quadrature rule

to discretize the singular integral in the radial direction. Indeed, there are now many techniques for discretizing the 1D singular to very high order. Standard texts on numerical integration [23] contain classical techniques such as production integration, integration by parts, and classical Gaussian quadratures. More recent developments include the hybrid Gauss-trapezoidal rule [2] and generalized Gaussian quadratures (see, for example, [16, 49]).

Remark 3.6. In summary, the error of the algorithm consists of three parts: (1) the truncation error in the Fourier domain which decays spectrally quickly for smooth data [63]; (2) the discretization error (or the quadrature error), which also decays spectrally fast for smooth data [23]; and (3) the interpolation error in NUFFT which can be made arbitrarily small [43]. All these error estimates are standard, and we omit details here.

4. Numerical examples. We have implemented the algorithms above in Fortran. For convenience, we have used the publicly available software package [44]. We used the gcc compiler (version 4.8.1) with option -O3 on a 64 bit linux workstation with a 2.93GHz Intel Xeon CPU and 12 Mb of cache. We restrict our attention to the performance of Algorithm 2.

For testing purposes, we have chosen right-hand sides (densities) for which the analytical solutions are known. In the following tables, the first column lists the total number of points in physical space; the second column lists the value of the parameter *prec*. In 2D problems, $prec = 0$ implies that the oversampling factor for the regular FFT is 2 and a 40×40 polar grid is used for the NUFFT. $prec = 1$ implies that the oversampling factor for the regular FFT is 3 and a 60×60 polar grid is used for the NUFFT. For 3D problems, $prec = 0$ implies that the oversampling factor for the regular FFT is 2 and a $24 \times 24 \times 24$ spherical grid is used for the NUFFT. $prec = 1$ implies that the oversampling factor for the regular FFT is 2 and a $40 \times 40 \times 40$ spherical grid is used for the NUFFT. The third column lists the time spent using the regular grid and the FFT. The fourth column lists the time spent on the irregular grid and the NUFFT. The fifth column lists the total time expended by the algorithm. All times are measured in seconds. Finally, the last column lists the relative L^2 error as compared with the analytical solution on a uniform grid in physical space.

Example 1 (Coulomb interactions in 2.5 dimensions). We take $d = 2$, $U(\mathbf{x}) = U_{\mathrm{Cou}}(\mathbf{x}) = \frac{1}{2\pi|\mathbf{x}|}$ as in (1.4), and $\rho(\mathbf{x}) = e^{-|\mathbf{x}|^2/a}$ with a a positive constant in (1.1). The analytical solution to (1.1) is given by the formula

$$u(\mathbf{x}) = \frac{\sqrt{\pi a}}{2} e^{-|\mathbf{x}|^2/2a} I_0\left(\frac{|\mathbf{x}|^2}{2a}\right), \qquad \mathbf{x} \in \mathbb{R}^2, \tag{4.1}$$

where I_0 is the modified Bessel function of order 0 (see, for example, [1]). The numerical solution is computed by the formula (1.16) with $d = 2$ via Algorithm 2. Table 1 lists the numerical results for $a = 1.3$.

Example 2 (dipole-dipole Interactions with the same dipole orientation in 2.5 dimensions). Here we take $d = 2$, $U(\mathbf{x})$ as in (1.7) with $\alpha = 0$ and $n_3 = 0$, and $\rho(\mathbf{x}) = e^{-|\mathbf{x}|^2/a}$ with a a positive constant in (1.1). The analytical solution to (1.1) is given by the formula

$$u(\mathbf{x}) = \frac{3\sqrt{\pi} e^{-r}}{4\sqrt{a}} \left[I_1(r) - I_0(r) + \frac{(\mathbf{x} \cdot \mathbf{n}_\perp)^2}{a} \left(2I_0(r) - \frac{1+2r}{r} I_1(r) \right) \right], \quad \mathbf{x} \in \mathbb{R}^2, \tag{4.2}$$

where $r = \frac{|\mathbf{x}|^2}{2a}$, $\mathbf{n}_\perp = (n_1, n_2)^T$, and I_1 is the modified Bessel function of order 1

TABLE 1
Error and timing results for Example 1.

N	*Prec*	T_{FFT}	T_{NUFFT}	T_{Total}	E
1024	0	0.10e-2	0.5e-2	0.60e-2	1.90e-8
4096	0	0.20e-2	0.60e-2	0.80e-2	1.57e-8
16438	0	0.10e-1	0.11e-1	0.21e-1	1.52e-8
65536	0	0.35e-1	0.30e-1	0.65e-1	1.50e-8
1024	1	0.20e-2	0.11e-1	0.13e-1	2.40e-11
4096	1	0.60e-2	0.12e-1	0.18e-1	3.84e-15
16438	1	0.20e-1	0.17e-1	0.37e-1	5.75e-15
65536	1	0.83e-1	0.37e-1	0.12	1.24e-14

(see, for example, [1]). The numerical solution is computed by the formula (1.16) with $d = 2$ via Algorithm 2. Table 2 lists the numerical results with $a = 1.3$ and a randomly selected orientation vector $\mathbf{n}_\perp = (0.52460, -0.85135)^T$.

TABLE 2
Error and timing results for Example 2.

N	*Prec*	T_{FFT}	T_{NUFFT}	T_{Total}	E
1024	0	0.10e-2	0.4e-2	0.50e-2	1.21e-6
4096	0	0.30e-2	0.60e-2	0.90e-2	9.33e-7
16438	0	0.10e-1	0.11e-1	0.21e-1	8.15e-7
65536	0	0.33e-1	0.31e-1	0.65e-1	8.67e-7
1024	1	0.30e-2	0.10e-1	0.13e-1	1.80e-8
4096	1	0.60e-2	0.12e-1	0.18e-1	1.05e-14
16438	1	0.20e-1	0.17e-1	0.37e-1	1.24e-14
65536	1	0.83e-1	0.37e-1	0.12	1.74e-14

Example 3 (dipole-dipole interactions with different dipole orientations in 2.5 dimensions). We take $d = 2$, $U(\mathbf{x})$ as (1.11) with $\alpha = 0$, $n_3 = 0$, and $m_3 = 0$, and $\rho(\mathbf{x}) = e^{-|\mathbf{x}|^2/a}$ with a a positive constant in (1.1). The analytical solution to (1.1) is given by the formula

$$u(\mathbf{x}) = \frac{3\sqrt{\pi}e^{-r}}{4\sqrt{a}}\left[(\mathbf{n}_\perp \cdot \mathbf{m}_\perp)(I_1(r) - I_0(r)) + \frac{(\mathbf{x}\cdot\mathbf{n}_\perp)(\mathbf{x}\cdot\mathbf{m}_\perp)}{a}\left(2I_0(r) - \frac{1+2r}{r}I_1(r)\right)\right],$$

where $r = \frac{|\mathbf{x}|^2}{2a}$ and $\mathbf{m}_\perp = (m_1, m_2)^T$. The numerical solution is computed by the formula (1.16) with $d = 2$ via the Algorithm 2. Table 3 shows the numerical results with $a = 1.8$, and randomly selected orientation vectors $\mathbf{n}_\perp = (-0.44404, -0.89600)^T$ and $\mathbf{m}_\perp = (0.85125, -0.52476)^T$.

TABLE 3
Error and timing results for Example 3.

N	*Prec*	T_{FFT}	T_{NUFFT}	T_{Total}	E
1024	0	0.10e-2	0.3e-2	0.40e-2	1.43e-6
4096	0	0.30e-2	0.60e-2	0.90e-2	1.36e-6
16438	0	0.90e-2	0.11e-1	0.20e-1	9.99e-7
65536	0	0.34e-1	0.31e-1	0.65e-1	7.59e-7
1024	1	0.30e-2	0.10e-1	0.13e-1	2.40e-8
4096	1	0.60e-2	0.12e-1	0.18e-1	1.06e-14
16438	1	0.21e-1	0.17e-1	0.38e-1	1.16e-14
65536	1	0.83e-1	0.37e-1	0.12	1.88e-14

Example 4 (Coulomb interactions in three dimensions). We take $d = 3$, $U(\mathbf{x}) =$

$U_{\mathrm{Cou}}(\mathbf{x}) = \frac{1}{4\pi|\mathbf{x}|}$ as (1.3), and $\rho(\mathbf{x})$ as

$$\rho(\mathbf{x}) = \left[-2\beta + 4\left(\frac{x^2}{a_1^2} + \frac{y^2}{a_2^2} + \frac{z^2}{a_3^2}\right)\right] e^{-g(\mathbf{x})}, \quad g(\mathbf{x}) = \frac{x^2}{a_1} + \frac{y^2}{a_2} + \frac{z^2}{a_3}, \tag{4.3}$$

where $\mathbf{x} = (x, y, z)^T$ and $\beta = \frac{1}{a_1} + \frac{1}{a_2} + \frac{1}{a_3}$ with a_1, a_2, and a_3 three positive constants in (1.1). The analytical solution to (1.1) is given by the formula

$$u(\mathbf{x}) = -e^{-g(\mathbf{x})} = -e^{-(x^2/a_1 + y^2/a_2 + z^2/a_3)}, \qquad \mathbf{x} = (x, y, z)^T \in \mathbb{R}^3. \tag{4.4}$$

The numerical solution is computed by the formula (1.16) with $d = 3$ via Algorithm 2. Table 4 depicts the numerical results for $a_1 = 1.0$, $a_2 = 1.3$, and $a_3 = 1.5$.

TABLE 4
Error and timing results for Example 4.

N	*Prec*	T_{FFT}	T_{NUFFT}	T_{Total}	E
32768	0	0.35e-1	1.04	1.07	2.84e-9
262144	0	0.75	1.56	2.31	2.51e-9
2097152	0	5.88	5.06	10.95	2.47e-9
16777216	0	48.98	34.98	84.07	2.46e-9
32768	1	0.36e-1	4.65	4.69	9.06e-10
262144	1	0.75	5.70	6.45	8.72e-14
2097152	1	5.93	9.42	15.36	8.53e-14
16777216	1	49.92	49.98	100.00	8.51e-14

Example 5 (dipole-dipole interactions with the same dipole orientation in three dimensions). We take $d = 3$, with $U(\mathbf{x})$ given by (1.7) and $\rho(\mathbf{x})$ given by (4.3) in (1.1). The analytical solution to (1.1) is given by the formula

$$u(\mathbf{x}) = -\rho(\mathbf{x}) + 6\left[2g_{\mathbf{n}}(\mathbf{x})^2 - \left(\frac{n_1^2}{a_1} + \frac{n_2^2}{a_2} + \frac{n_3^2}{a_3}\right)\right] e^{-g(\mathbf{x})}, \quad g_{\mathbf{n}}(\mathbf{x}) = \frac{xn_1}{a_1} + \frac{yn_2}{a_2} + \frac{zn_3}{a_3}.$$

The numerical solution is computed by the formula (1.16) with $d = 3$ via Algorithm 2. Table 5 lists the numerical results for $a_1 = 1.3$, $a_2 = 1.5$, $a_3 = 1.8$, and randomly selected orientation vector $\mathbf{n} = (-0.36589, -0.69481, 0.61916)^T$.

TABLE 5
Error and timing results for Example 5.

N	*Prec*	T_{FFT}	T_{NUFFT}	T_{Total}	E
32768	0	0.36e-1	1.04	1.08	3.06e-7
262144	0	0.75	1.55	2.30	1.15e-7
2097152	0	5.84	5.07	10.93	3.81e-8
16777216	0	50.53	35.77	86.39	1.13e-7
32768	1	0.37e-1	4.65	4.69	2.65e-7
262144	1	0.75	5.70	6.44	1.13e-13
2097152	1	5.90	9.39	15.30	1.12e-13
16777216	1	50.53	49.38	100.01	8.67e-14

Example 6 (dipole-dipole interactions with different dipole orientations in three dimensions). We take $d = 3$, with $U(\mathbf{x})$ given by (1.11) with $\alpha = 0$, and $\rho(\mathbf{x})$ given by (4.3) in (1.1). The analytical solution to (1.1) is given by the formula

$$u(\mathbf{x}) = -\rho(\mathbf{x}) + 6\left[2g_{\mathbf{n}}(\mathbf{x})g_{\mathbf{m}}(\mathbf{x}) - \left(\frac{n_1m_1}{a_1} + \frac{n_2m_2}{a_2} + \frac{n_3m_3}{a_3}\right)\right] e^{-g(\mathbf{x})}, \quad \mathbf{x} \in \mathbb{R}^3. \tag{4.5}$$

The numerical solution is computed by the formula (1.16) with $d = 3$ via Algorithm 2. Table 6 shows the numerical results for $a_1 = 1.2$, $a_2 = 1.45$, $a_3 = 1.73$, $\mathbf{n} = (0.82778, 0.41505, -0.37751)^T$, and $\mathbf{m} = (0.31180, 0.93780, -0.15214)^T$.

TABLE 6
Error and timing results for Example 6.

N	$Prec$	T_{FFT}	T_{NUFFT}	T_{Total}	E
32768	0	0.36e-1	1.04	1.08	3.18e-7
262144	0	0.75	1.55	2.30	1.59e-7
2097152	0	5.92	5.11	11.04	8.28e-8
16777216	0	50.20	35.80	86.09	1.53e-7
32768	1	0.36e-1	4.65	4.69	3.36e-7
262144	1	0.75	5.70	6.46	1.00e-13
2097152	1	5.88	9.36	15.26	3.90e-13
16777216	1	50.34	42.36	92.79	1.04e-13

Example 7 (the interaction energy of dipole-dipole interactions with the same dipole orientation in three dimensions). We take $d = 3$, with $U(\mathbf{x})$ given by (1.7) and $\mathbf{n} = (0, 0, 1)^T$ and $\rho(\mathbf{x})$ given by

$$\rho(\mathbf{x}) = \pi^{-3/2}\gamma_x\sqrt{\gamma_z}e^{-(\gamma_x(x^2+y^2)+\gamma_z z^2)}, \qquad \mathbf{x} = (x, y, z)^T \in \mathbb{R}^3, \tag{4.6}$$

with γ_x, γ_y, and γ_z three positive constants, in (1.1). The dipole-dipole interaction energy $E(\rho)$ in (1.2) can be evaluated analytically as [5, 54, 61, 62]

$$E(\rho) = -\frac{\lambda\gamma_x\sqrt{\gamma_z}}{4\pi\sqrt{2\pi}} \begin{cases} \dfrac{1+2\kappa^2}{1-\kappa^2} - \dfrac{3\kappa^2 \arctan\sqrt{\kappa^2-1}}{(1-\kappa^2)\sqrt{\kappa^2-1}}, & \kappa > 1, \\ 0, & \kappa = 1, \\ \dfrac{1+2\kappa^2}{1-\kappa^2} - \dfrac{3\kappa^2}{2(1-\kappa^2)\sqrt{1-\kappa^2}} \ln\left(\dfrac{1+\sqrt{1-\kappa^2}}{1-\sqrt{1-\kappa^2}}\right), & \kappa < 1, \end{cases} \tag{4.7}$$

where $\kappa = \sqrt{\gamma_z/\gamma_x}$. Three cases with $\lambda = 8\pi/3$ are considered here.

Case I. $\gamma_x = 0.25$ and $\gamma_z = 1$; the exact energy is $E(\rho) \approx 0.03867086140999021$;

Case II. $\gamma_x = 1$ and $\gamma_z = 1$; the exact energy is $E(\rho) = 0$;

Case III. $\gamma_x = 2$ and $\gamma_z = 1$; the exact energy is $E(\rho) \approx -0.1386449740987819$.

The energy is computed numerically by the formula (1.16) with $d = 3$ via Algorithm 2 (see Remark 3.3 as well). Table 7 shows the numerical results for the above three cases. From this table, we observe that our algorithm achieves full double precision, while at most seven digit accuracy is achieved in [5].

Remark 4.1. From these tables, it is clear that the timing scales roughly linearly with N. The timing difference between $prec = 0$ and $prec = 1$ is not very significant. Thus, we recommend setting $prec = 1$ in general.

5. Conclusions. An efficient and high-order algorithm has been constructed for the evaluation of long-range Coulomb and dipole-dipole interactions of the type which arise in quantum physics and chemistry as well as materials simulation and design. The algorithm evaluates these interactions in the Fourier domain with a coordinate transformation that removes the singularity at the origin. The Fourier integral is then discretized via high-order accurate quadrature, and the resulting discrete summation is carried out using the nonuniform FFT (NUFFT). The algorithm is straightforward

TABLE 7

Numerical results for computing the dipole-dipole interaction energy in three dimensions. Here N is the total number of points in the computational domain, N_I is the total number of irregular points in the Fourier domain, E_c is the computed value of the dipole-dipole interaction energy, $E := |E_c - E(\rho)|$ is the absolute error when $E(\rho) = 0$ (Case II*), $E := |E_c - E(\rho)|/|E(\rho)|$ is the relative error when $E(\rho) \neq 0$ (Cases* I *and* III*), and T is the total CPU time in seconds.*

	N	N_I	E_c	E	T
Case I	32768	1000	0.03867932878216508	2.3e-4	0.14
	32768	3375	0.03867085889326449	6.6e-8	0.25
	262144	8000	0.03867086140931093	1.8e-11	1.12
	262144	27000	0.03867086140998955	1.8e-14	1.89
Case II	32768	1000	-4.096001975539615e-7	4.1e-7	0.14
	32768	3375	1.983944760166238e-9	2.0e-9	0.23
	262144	8000	5.117228774684975e-14	5.1e-14	1.19
	262144	27000	-7.785768552598901e-16	7.8e-16	1.87
Case III	32768	1000	−0.1386463326990541	1.0e-5	0.14
	32768	3375	−0.1386449725315638	1.2e-8	0.20
	262144	8000	−0.1386449740987009	5.8e-13	1.12
	262144	27000	−0.1386449740987584	1.7e-13	1.84

to implement and requires $O(N \log N)$ operations, where N is the total number of points in the physical space discretization. Thus, the net cost is of the same order as that of using the uniform FFT for problems with periodic boundary conditions. Our algorithm is easily extended to the computation of any nonlocal interaction that has a suitable convolution structure. When the singularity in the Fourier transform cannot be accounted for by a simple change of variables, generalized Gaussian quadrature can be used to create a high-order discretization [16, 49], to which the NUFFT can be applied, achieving nearly optimal computational complexity. An example where this extension of our algorithm is helpful is the solution of the free space Poisson equation in two dimensions, where the Fourier transform of the kernel is $\frac{1}{\|\mathbf{k}\|^2}$ and the integrand is still singular after switching to polar coordinates. We plan to incorporate the method described here into efficient and accurate solvers for computing the ground state and dynamics of dipolar BECs, the nonlinear Schödinger equation with a Coulomb potential, and the Kohn–Sham equations for electronic structure. Similar ideas have been used for computing Stokes interactions with compactly supported data with a mixture of free space and periodic boundary conditions imposed on a unit cell [46, 47].

Acknowledgments. The authors would like to thank Mark Tygert and Anna-Karin Tornberg for many useful discussions.

REFERENCES

[1] M. ABRAMOWITZ AND I. A. STEGUN, *Handbook of Mathematical Functions*, Dover, New York, 1965.

[2] B. K. ALPERT, *Hybrid Gauss-trapezoidal quadrature rules*, SIAM J. Sci. Comput., 20 (1999), pp. 1551–1584.

[3] W. BAO, N. BEN ABDALLAH, AND Y. CAI, *Gross–Pitaevskii–Poisson equations for dipolar Bose–Einstein condensate with anisotropic confinement*, SIAM J. Math. Anal., 44 (2012), pp. 1713–1741.

[4] W. BAO AND Y. CAI, *Mathematical theory and numerical methods for Bose-Einstein condensation*, Kinet. Relat. Mod., 6 (2013), pp. 1–135.

[5] W. BAO, Y. CAI, AND H. WANG, *Efficient numerical methods for computing ground states and dynamics of dipolar Bose-Einstein condensates*, J. Comput. Phys., 229 (2010), pp. 7874–7892.

[6] W. Bao, D. Jaksch, and P. A. Markowich, *Numerical solution of the Gross-Pitaevskii equation for Bose-Einstein condensation*, J. Comput. Phys., 187 (2003), pp. 318–342.
[7] W. Bao, S. Jin, and P. A. Markowich, *On time-splitting spectral approximation for the Schrödinger equation in the semiclassical regime*, J. Comput. Phys., 175 (2002), pp. 487–524.
[8] W. Bao, H. Jian, N. J. Mauser, and Y. Zhang, *Dimension reduction of the Schrödinger equation with Coulomb and anisotropic confining potentials*, SIAM J. Appl. Math., 73 (2013), pp. 2100–2123.
[9] W. Bao, D. Marahrens, Q. Tang, and Y. Zhang, *A simple and efficient numerical method for computing the dynamics of rotating Bose–Einstein condensates via rotating Lagrangian coordinates*, SIAM J. Sci. Comput., 35 (2013), pp. A2671–A2695.
[10] W. Bao, N. J. Mauser, and H. P. Stimming, *Effective one particle quantum dynamics of electrons: A numerical study of the Schrödinger-Poisson-Xα model*, Commun. Math. Sci., 1 (2003), pp. 809–831.
[11] C. Bardos, L. Erdős, F. Golse, N. J. Mauser, and H.-T. Yau, *Derivation of the Schrödinger-Poisson equation from the quantum N-particle Coulomb problem*, C. R. Math. Acad. Sci. Paris, 334 (2002), pp. 515–520.
[12] C. Bardos, F. Golse, and N. J. Mauser, *Weak coupling limit of the N-particle Schrödinger equation*, Methods Appl. Anal., 7 (2000), pp. 275–293.
[13] N. Ben Abdallah, F. Castella, F. Delebecque-Fendt, and F. Méhats, *The strongly confined Schrödinger–Poisson system for the transport of electrons in a nanowire*, SIAM J. Appl. Math., 69 (2009), pp. 1162–1173.
[14] G. Beylkin, *On the fast Fourier transform of functions with singularities*, Appl. Comput. Harmon. Anal., 2 (1995), pp. 363–383.
[15] P. B. Blakie, C. Ticknor, A. S. Bradley, A. M. Martin, M. J. Davis, and Y. Kawaguchi, *Numerical method for evolving the dipolar projected Gross-Pitaevskii equation*, Phys. Rev. E, 80 (2009), 016703.
[16] J. Bremer, Z. Gimbutas, and V. Rokhlin, *A nonlinear optimization procedure for generalized Gaussian quadratures*, SIAM J. Sci. Comput., 32 (2010), pp. 1761–1788.
[17] Y. Cai, M. Rosenkranz, Z. Lai, and W. Bao, *Mean-field regime of trapped dipolar Bose-Einstein condensates in one and two dimensions*, Phys. Rev. A, 82 (2010), 043623.
[18] R. Carles, P. A. Markowich, and C. Sparber, *On the Gross-Pitaevskii equation for trapped dipolar quantum gases*, Nonlinearity, 21 (2008), pp. 2569–2590.
[19] H. Cheng, L. Greengard, and V. Rokhlin, *A fast adaptive multipole algorithm in three dimensions*, J. Comput. Phys., 155 (1999), pp. 468–498.
[20] B. Cichocki and B. U. Felderhof, *Electrostatic interactions in thin-film Coulomb systems with periodic boundary conditions*, Molecular Phys., 67 (1989), pp. 1373–1384.
[21] J. W. Cooley and J. W. Tukey, *An algorithm for the machine calculation of complex Fourier series*, Math. Comput., 19 (1965), pp. 297–301.
[22] A. Dutt and V. Rokhlin, *Fast Fourier transforms for nonequispaced data*, SIAM J. Sci. Comput., 14 (1993), pp. 1368–1393.
[23] P. J. Davis and P. Rabinowitz, *Methods of Numerical Integration*, Academic Press, New York, 1975.
[24] A. Dutt and V. Rokhlin, *Fast Fourier transforms for nonequispaced data.* II, Appl. Comput. Harmon. Anal., 2 (1995), pp. 85–100.
[25] H. Fehske, R. Schneider, and A. Weiße, *Computational Many-Particle Physics*, Lecture Notes in Phys. 739, Springer, New York, 2008.
[26] J. A. Fessler and B. P. Sutton, *Nonuniform fast Fourier transforms using minmax interpolatio*, IEEE Trans. Signal Process., 51 (2003), pp. 560–574.
[27] K. Fourmont, *Non-equispaced fast Fourier transforms with applications to tomography*, IEEE Trans. Signal Process., 9 (2003), pp. 431–450.
[28] Z. Gimbutas, L. Greengard, and M. Minion, *Coulomb interactions on planar structures: Inverting the square root of the Laplacian*, SIAM J. Sci. Comput., 22 (2001), pp. 2093–2108.
[29] Z. Gimbutas and V. Rokhlin, *A generalized fast multipole method for nonoscillatory kernels*, SIAM J. Sci. Comput., 24 (2002), pp. 796–817.
[30] L. Greengard and J.-Y. Lee, *Accelerating the nonuniform fast Fourier transform*, SIAM Rev., 46 (2004), pp. 443–454.
[31] L. Greengard and V. Rokhlin, *A fast algorithm for particle simulations*, J. Comput. Phys., 73 (1987), pp. 325–348.
[32] L. Greengard and V. Rokhlin, *A new version of the fast multipole method for the Laplace equation in three dimensions*, Acta Numer., 6 (1997), pp. 229–269.

[33] A. Griesmaier, J. Werner, S. Hensler, J. Stuhler, and T. Pfau, *Bose-Einstein condensation of chromium*, Phys. Rev. Lett., 94 (2005), 160401.
[34] H. Haken, W. D. Brewer, and H. C. Wolf, *Molecular Physics and Elements of Quantum Chemistry*, Springer, New York, 1995.
[35] R. A. James, *The solution of Poisson equation for isolated source distributions*, J. Comput. Phys., 25 (1977), pp. 71–93.
[36] F. John, *Partial Differential Equations*, 4th ed., Springer, New York, 1982.
[37] M. Kiffer, H. Park, W. Li, and T. F. Gallagher, *Dipole-dipole-coupled double-Rydberg molecules*, Phys. Rev. A, 86 (2012), 031401(R).
[38] M. Kiffer, W. Li, and D. Jaksch, *Magnetic monopoles and synthetic spin-orbit coupling in Rydberg marcrodimers*, Phys. Rev. Lett., 110 (2013), 170402.
[39] M. Kiffer, W. Li, and D. Jaksch, *Abelian and non-Abelian gauge fields in dipole-dipole interacting Rydberg atoms*, J. Phys. B, 46 (2013), 134008.
[40] W. Kohn and L. J. Sham, *Self-consistent equations including exchange and correlation effects*, Phys. Rev., 140 (1965), pp. 1133–1138.
[41] P. Mccorquodale, P. Colella, G. T. Balls, and S. B. Baden, *A scalable parallel Poisson solver in three dimensions with infinite-domain boundary conditions*, in Proceedings of the 7th International Workshop on High Performance Scientific and Engineering Computing, Oslo, Norway, 2005, pp. 814–822.
[42] T. Lahaye, C. Menotti, L. Santos, M. Lewenstein, and T. Pfau, *The physics of dipolar bosonic quantum gases*, Rep. Progr. Phys., 72 (2009), 126401.
[43] J. Y. Lee and L. Greengard, *The type* 3 *nonuniform FFT and its applications*, J. Comput. Phys., 206 (2005), pp. 1–5.
[44] J. Y. Lee, L. Greengard, and Z. Gimbutas, *NUFFT Version* 1.2 *Software Release*, available from http://www.cims.nyu.edu/cmcl/nufft/nufft.html.
[45] M. H. Levitt, *Spin Dynamics: Basics of Nuclear Magnetic Resonance*, Wiley, New York, 2008.
[46] D. Lindbo and A.-K. Tornberg, *Spectral accuracy in fast Ewald-based methods for particle simulations*, J. Comput. Phys., 230 (2011), pp. 8744–8761.
[47] D. Lindbo and A.-K. Tornberg, *Fast and spectrally accurate Ewald summation for* 2*-periodic electrostatic systems*, J. Chem. Phys., 136 (2012), 164111.
[48] M. Lu, N. Q. Burdick, S.-H. Youn, and B. L. Lev, *A strongly dipolar Bose-Einstein condensate of dysprosium*, Phys. Rev. Lett., 107 (2011), 190401.
[49] J. Ma, V. Rokhlin, and S. Wandzura, *Generalized Gaussian quadrature rules for systems of arbitrary functions*, SIAM J. Numer. Anal., 33 (1996), pp. 971–996.
[50] T. Miyakawa, T. Sogo, and H. Pu, *Phase-space deformation of a trapped dipolar Fermi gas*, Phys. Rev. A, 77 (2008), 061603(R).
[51] D. H. J. O′Dell, S. Giovanazzi, and C. Eberlein, *Exact hydrodynamics of a trapped dipolar Bose-Einstein condensate*, Phys. Rev. Lett., 92 (2004), 250401.
[52] D. H. O′Dell and C. Eberlein, *Vortex in a trapped Bose-Einstein condensate with dipole-dipole interactions*, Phys. Rev. A, 75 (2007), 013604.
[53] D. Potts, G. Steidl, and M. Tasche, *Fast Fourier transforms for nonequispaced data: A tutorial*, in Modern Sampling Theory, Appl. Numer. Harmon. Anal., J. J. Benedetto and P. Ferreira, eds., Birkhäuser, Boston, 2001, pp. 247–270.
[54] N. G. Parker, C. Ticknor, A. M. Martin, and D. H. J. O'Dell, *Structure formation during the collapse of a dipolar atomic Bose-Einstein condensate*, Phys. Rev. A, 79 (2009), 013617.
[55] R. G. Parr and W. Yang, *Density-Functional Theory of Atoms and Molecules*, Oxford University Press, Oxford, UK, 1989.
[56] M. Rosenkranz, Y. Cai, and W. Bao, *Effective dipole-dipole interactions in multilayered dipolar Bose-Einstein condensates*, Phys. Rev. A, 88 (2013), 013616.
[57] L. Santos, G. Shlyapnikov, P. Zoller, and M. Lewenstein, *Bose-Einstein condensation in trapped dipolar gases*, Phys. Rev. Lett., 85 (2000), pp. 1791–1797.
[58] D. E. Sheely and J. Schmalian, *Quantum critical scaling in graphene*, Phys. Rev. Lett., 99 (2007), 226803.
[59] D. E. Sheely and J. Schmalian, *Optical transparency of graphene as determined by the fine structure constant*, Phys. Rev. B, 80 (2009), 193411.
[60] G. Strang, *Introduction to Linear Algebra*, 4th ed., Wellesley-Cambridge Press, Wellesley, MA, 2009.
[61] C. Ticknor, N. G. Parker, A. Melatos, S. L. Cornish, D. H. J. O'Dell, and A. M. Martin, *Collapse times of dipolar Bose-Einstein condensates*, Phys. Rev. A, 78 (2008), 061607.

[62] I. Tikhonenkov, B. A. Malomed, and A. Vardi, *Anisotropic solitons in dipolar Bose-Einstein condensates*, Phys. Rev. Lett., 100 (2008), 090406.
[63] L. N. Trefethen, *Spectral Methods in MATLAB*, SIAM, Philadelphia, 2000.
[64] B. Xiong, J. Gong, H. Pu, W. Bao, and B. Li, *Symmetry breaking and self-trapping of a dipolar Bose-Einstein condensate in a double-well potential*, Phys. Rev. A, 79 (2009), 013626.
[65] S. Yi and H. Pu, *Vortex structures in dipolar condensates*, Phys. Rev. A, 73 (2006), 061602.
[66] S. Yi and L. You, *Trapped atomic condensates with anisotropic interactions*, Phys. Rev. A, 61 (2000), 041604.
[67] S. Yi and L. You, *Trapped condensates of atoms with dipole interactions*, Phys. Rev. A, 63 (2001), 053607.
[68] L. Ying, G. Biros, and D. Zorin, *A kernel-independent adaptive fast multipole algorithm in two and three dimensions*, J. Comput. Phys., 196 (2004), pp. 591–626.
[69] Y. Zhang and X. Dong, *On the computation of ground state and dynamics of Schrödinger-Poisson-Slater system*, J. Comput. Phys., 230 (2011), pp. 2660–2676.